Trends in Biomaterials and Artificial Organs
www.biomaterials.org.in/tibao
ISSN 0971-1198
https://doi.org/10.5281/zenodo.16957128

Original Article

Evaluation of the Structural Integrity and Functionality of a Stance Control Knee Ankle Foot Orthosis Knee Joint Using Experimental and Computational Approaches

Akash Steephen[1], S. Sumith[2], N.R. Rajesh[1], N.N. Subhash[2*], Renjith Sasi[3], M. Abhijith[2], Vishnu S. Prasad[2], C.V. Muraleedharan[2]

[1]*Department of Mechanical Engineering, College of Engineering Trivandrum, India*
[2]*Department of Medical Devices Engineering,* [3]*Department of Technology and Quality Management, Biomedical Technology Wing, Sree Chitra Tirunal Institute for Medical Sciences and Technology, Thiruvananthapuram 695012, India*

Received: *2 June 2025*
Accepted: *22 July 2025*
Published online: *26 August 2025*

Keywords: *stance control orthosis, finite element analysis, ground reaction force, assistive device, lower limb orthosis*

Walking is an essential part of daily mobility, but individuals with conditions such as polio, muscle weakness, spinal cord injuries, or multiple sclerosis often depend on Knee-Ankle-Foot Orthoses (KAFO) that keep the knee locked throughout both the stance and swing phases of walking. This restriction leads to abnormal gait patterns, increased joint stress on the hip and lower back, and a reduction in gait efficiency. To overcome these drawbacks, Stance-Control-Knee-Ankle -Foot-Orthosis (SCKAFO) has been developed, offering knee support during the stance phase and permitting knee movement during the swing phase. This study presents a combined *in silico* and experimental analysis of a mechanical SCKAFO using a commercially available predicate device. Experiments were conducted to evaluate the unlocking forces of the knee joint. To replicate the rigid body dynamics behaviour of the orthosis, a simplified 3D CAD model was created, and the results of rigid body dynamics match the experimental findings. Also, the structural response of the orthosis knee joint under both theoretical and actual loading scenarios was examined using finite element analysis. *In silico* results shows that the orthosis knee joint is structurally safe under the worst loading condition. The validated simplified 3D CAD model demonstrated close agreement with experimental results, showing deviations of 3.96 % at the pawl cable and 2.61 % at the foot loading. It revealed equivalent von Mises stresses of 8.63 MPa under theoretical loading and 4.70 MPa under practical loading, underscoring the potential of analysis-driven design to advance next-generation mechanical SCKAFO knee joint development, despite minor variations from cable dynamics and model simplifications.

Introduction

Approximately 1.5% of the world's population may require prosthetic and orthotic interventions for their mobility and well-being. However, only 5–15% of those in need have access to these assistive devices [1]. Among them, individuals with lower limb impairments caused by polio, weak muscles, paralysis, spinal injuries, and neurological conditions often rely on orthotic solutions such KAFOs. KAFOs are orthotic devices that provide support and prevent the knee from collapsing. However, a major limitation of KAFOs is that they keep the knee locked during all phases of gait. Walking with a fixed knee can result in a 24% reduction in gait efficiency and lead to a significant increase in the vertical displacement of the centre of mass by up to 65%, which causes strain on the hip joint and lower back, leading to pain and discomfort [2]. To address these limitations, a new type of orthosis, called the SKAFOs, has been developed. Unlike traditional KAFOs, the SCKAFOs are designed to allow free knee movement during the swing phase of walking while arresting knee flexion during the stance phase, thereby enabling a more natural and efficient gait [2].

SCKAFO can be generally categorized into three types based on the mechanism used to lock and unlock the knee: Mechanical, Electronic, and Microprocessor type SCKAFO [3]. The mechanical SCKAFO operates through either ankle movement or gravity to control the knee's locking mechanism. In some designs, ankle

* *Coresponding author*
E-mail address: nnsubhash@gmail.com (*Er. N.N. Subhash, Scientist D, Department of Medical Devices Engineering, Biomedical Technology Wing, Sree Chitra Tirunal Institute for Medical Sciences and Technology, Thiruvananthapuram 695012, India*)

movement activates a spring-loaded pawl that locks and unlocks the knee during the swing and stance phases of gait [2]. In other versions, a gravity-actuated mechanism is used, where a weighted pawl moves in and out of the locking position based on the user's thigh angle, enabling knee locking during stance and free motion during swing [3]. The electronic SCKAFO utilizes various sensors to control the knee joint. Force or pressure sensors at the foot detect load changes to lock or unlock the knee, while a gyroscope measures step length and pre-locks the knee during terminal swing, fully locking it upon complete knee extension. Additionally, motion sensors track the deceleration of the leg, triggering the knee to lock for stability [3, 4]. C-Brace (M/s. Ottobock, Germany) is an example of the microprocessor type SCKAFO. It incorporates a carbon fibre support structure along with sensors that detect ankle moment and a knee joint controlled by a monocentric mechanism. A sensor tracks knee angle to monitor both the position and speed of knee movement. The system modulates flexion and extension resistance through a microprocessor that operates at a frequency of 50 Hz, using data such as ankle force, knee angle, knee motion velocity, and hydraulic system temperature [5].

The SCKAFO consists of a thigh shell for upper leg support, a calf shell for lower leg support, and a foot plate to provide weight distribution and balance. The ankle component, which may be standard action, double action, or dorsiflexion assist, varies based on the knee joint mechanism and the user's medical needs. The knee joint provides flexion during the swing phase and ensures stability during the stance phase. The stirrups connect the ankle component to the foot plate. The uprights are rigid structural elements that connect the thigh shell, calf shell, knee joint, and ankle component. Design approach used in SCKAFO is modular architecture, which improves flexibility for modifications, simplifies the assembly process, and enables easy replacement of individual components without affecting the overall system. Material selection for the SCKAFO plays a pivotal role in determining the device's performance, comfort, and durability. To provide a comprehensive overview, a summary of the key materials used for different components of the SCKAFO is presented in table1.

Major weight-bearing components are fabricated from materials such as stainless steel, titanium, or aluminium, with the selection depending on the user's body weight and specific load-bearing requirements. In SCKAFO with Becker FullStride knee joint (M/s. Becker Orthopedics, USA, Predicate device), stainless steel is the material used for the knee joint parts because of its strength and durability. These parts are usually made using CNC machining, which helps achieve precise shapes and dimensions. The uprights, which serve as the connecting elements between the knee joint and the orthotic shells, are manufactured from Stainless Steel and are shaped to match the natural contour and width of the leg, providing better fit and support. The thigh shell, calf shell, and foot plate are made from thermoplastic materials like polypropylene. These parts are usually made using vacuum forming process, which allows the material to take the shape of the user's limb for improved comfort and function.

Table 1: Materials used in SCKAFO from literature

No	Component	Materials	Ref
1	Thigh Shell	Polypropylene(PP), or carbon fibre	[23,20]
2	Calf Shell	Polypropylene(PP), or carbon fibre	[23,20]
3	Foot Plate	Polypropylene(PP), or carbon fibre	[23,20]
4	Ankle component	Stainless steel, Aluminium, or Titanium	[16,22]
5	Upper part, and lower part	Aluminium, Stainless Steel, or Titanium	[18,21]
6	Upright	Aluminium, Stainless Steel, or Titanium	[17,16]
7	Y Stirrups	Stainless Steel	[16]
8	Cable	Stainless Steel	[19]

Several studies have been conducted to understand the performance of KAFO and SCKAFO. These investigations are primarily focused on enhancing gait efficiency, reducing orthotic weight, improving user comfort, and analysing load distribution during ambulation. Jan Andrysek et al. investigated the biomechanical response of KAFOs during ambulation over irregular ground surfaces. To quantify the loading conditions experienced by the orthosis, a six-degree-of-freedom load cell was embedded at the lateral knee joint [6]. This setup enabled the measurement of forces and moments along all three anatomical axes. The acquired data were subsequently normalized to body mass, facilitating cross-subject comparison and broader applicability. The study's output, particularly the normalized force and moment profiles, has been frequently referenced in later works as boundary conditions for structural and dynamic analyses.

S F Khan et al. proposed a lightweight redesign of KAFOs utilizing additive manufacturing and topology optimization [7]. Their approach integrated Voronoi-based structural patterns to reduce material usage without compromising mechanical strength. Finite element simulations showed a reduction in both volume and maximum stress, demonstrating the feasibility of producing customized, structurally efficient KAFOs using 3D printing technologies. Importantly, the boundary conditions for the (finite element analysis) FEA analysis were derived from the normalized kinetic data reported by Andrysek et al [6]. SCKAFO aimed at paediatric users was developed by Lucas F. Gerez et al., focusing on child-specific needs [8]. Their proposed orthotic design uses a ratchet and pawl mechanism, offering knee support during the stance phase and permitting knee movement during the swing phase. The knee joint is designed to withstand the maximum internal knee joint moment generated while stair climbing, and also calculates the strap reaction force acting during one leg stance position. A key innovation in their work is the integration of a length-adjustable support structure, allowing the orthosis to accommodate growth from two to six years of age, thereby reducing the need for frequent replacements. Font-Llagunes et al. developed a simulation model of an active SCKAFO intended for individuals with incomplete spinal cord injury [9]. Their work employed a multibody dynamics framework along with static optimization to evaluate the interaction between muscular contributions and orthotic actuation. The resulting orthosis featured a powered knee unit capable of controlling flexion during swing and providing passive resistance during stance, tailored to the patient's neuromuscular condition. The study emphasized the importance of combining biomechanical modelling with actuator selection to enhance orthotic design.

This study was conducted as a benchmarking investigation to evaluate the rigid body dynamics behaviour, structural performance, and unlocking characteristics of a commercially available predicate device. Designed for individuals with lower limb impairments who possess a minimum muscle strength grade of 3, this orthosis was experimentally assessed to determine the load required to unlock the knee joint. To represent orthosis in simulations, simplified 3D CAD model of the predicate device was developed, and rigid body dynamics simulations were performed to replicate the experimental setups, thereby validating the model. In addition, a theoretical force analysis was carried out to estimate the worst-case loading on the

Figure 1: Predicate device used for the study

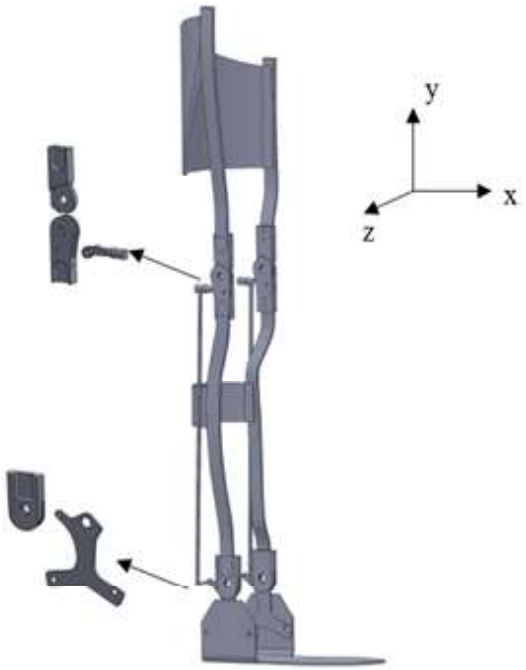

Figure 2: Simplified 3D CAD model used for investigation

Table 2: Assumptions and remarks

	Assumption	Basis for assumption	Risk	Implications of the assumption
1	Predicate device is represented as a simplified 3D model	The analysis emphasizes rigid body dynamics	Low	Minute surface features may not produce significant variations in this rigid body dynamics study
2	Weight of 60kg is considered for the analysis	Manufacturer's data sheet weight limit is =140lbs/ 63.5kg [17]	Low	The analysis scope is limited to a user weight of 60kg
3	4° of pawl rotation is considered for unlocking	Derived from experimental findings identifying this as the minimum angle for disengagement	Low	The model reliably estimated the unlocking force.
4	The position of the leg with orthosis is considered between heel strike and loading response.	In this phase, the ground reaction force is known to act posterior to the knee joint [14]	Low	Focus is maintained on critical stance phases: heel strike, mid-stance, and terminal stance.
5	The ground reaction force acts at a moment arm length of 44 mm from the knee joint.	Based on prior biomechanical studies [10]	Low	Facilitates estimation of the angle at which the ground reaction force acts with respect to leg
6	Maximum load is generated in the running condition	Running generates a higher ground reaction force than walking, often reaching up to 2 – 2.8 times the body weight [11]	Low	Allows determination of the orthosis maximum load-bearing capacity.
7	All inter-component connections are modelled as fixed, and pawl and cable are not considered to find the load at the knee joint during FEA.	To simplify analysis, connections are treated as rigid under static equilibrium, focusing on load transmission rather than joint flexibility.	Low	Allows the determination of load acting at knee joint in x, y, and z direction.
8	Maximum load transferred to the orthosis is between 30% to 83%	Based on prior studies [12]	Low	Allow estimation of range of load distribution

Figure 3: Experimental setup showing the load cell, force gauge, and the Predicate device mechanical knee joint. The yellow-highlighted point at the foot of the orthosis indicates the location where the load is applied

knee joint during running. Finally, static structural analyses using finite element methods were conducted under both theoretical and experimental loading conditions to evaluate the structural safety of the knee joint.

Methods

Predicate device and simplified 3D CAD model

Figure 1 shows the picture of predicate device, and figure 2 shows its simplified 3D CAD model. The measured weight of the predicate device is 2.3 kg. The key assumptions made during the theoretical calculations and simulations, are summarized in table 2.

Material identification of predicate device

Material identification and elemental analysis of the predicate device components were conducted using a handheld X-ray Fluorescence analyser (Model: X-200 SciAps, USA). The analysis was performed on the upper part, lower part, pawl, ankle component, and uprights to determine their elemental composition. Two experimental procedures were conducted to determine the unlocking load of the orthosis under different loading conditions.

Measurement of unlocking force via foot load application

In this experiment, predicate device was positioned on a stable, flat surface, and force was applied manually at the foot using a load cell (Model: ZTA-DPU-100N , IMADA, Japan), placed 180 mm from the ankle joint centre in upward direction. The applied force gradually increased until the pawl rotated by 4°, corresponding to the unlocking position. This procedure was repeated for a total of ten trials.

Measurement of unlocking force via direct cable loading

In this experiment (figure 3), the same setup was used, but the load was applied directly at the pawl cable point (35mm away from pivot point) instead of the foot as in the first experiment. Similar to the first experiment, the force was progressively increased until the pawl rotates by 4°, and the process was repeated for ten trials.

Rigid body analysis

Rigid body dynamics simulation was carried out to replicate the experimental tests and validate the simplified 3D CAD model of

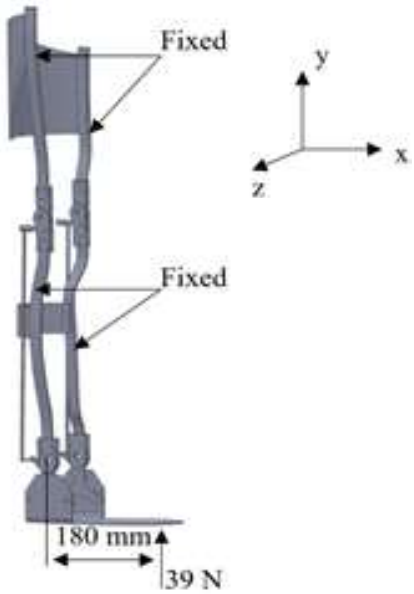

Figure 4: Boundary condition of the first rigid body dynamics model with vertical load applied at the foot

Figure 5: Boundary conditions of the second rigid body dynamics model with ankle–Y-stirrup rotation

Table 3:

No	Component	Materials	Justification
1	Thigh Shell	Polypropylene(PP)	[23]
2	Calf Shell	Polypropylene(PP)	[23]
3	Foot Plate	Polypropylene(PP)	[23]
4	Ankle Component	304 Stainless Steel	Experimentally measured
5	Upper part, lower part	410 Stainless Steel	Experimentally measured
6	Pawl	Fe 4140	Experimentally measured
7	Upright	304 Stainless Steel	[16],Experimentally measured
8	Y Stirrups	304 Stainless Steel	[16]
9	Cable	Stainless Steel	[19]

orthosis. Rigid body analysis of the virtual model was performed using ANSYS, simulating the unlocking behaviour under similar loading conditions used in the experiment.

In the ANSYS simulations, component connections were defined to replicate realistic joint. The Foot Plate was fixed to the Y Stirrup, providing a stable base. The y-Stirrup was connected to the Ankle Component via a rotational joint that allows movement around the z-axis, and a similar rotational connection was established between the Y Stirrup and the Steel Cable. The Thigh Shell and the Upper Part were rigidly fixed to the Upper Upright to ensure structural support. The Pawl was joined to the Steel Cable and the Lower Part through rotational joints, permitting controlled rotation about the z-axis. A rotational joint also connects the Upper and Lower Parts, enabling knee flexion. The Calf Shell and the Lower Part were rigidly fixed to the Lower Upright to ensure structural support. The model included a torsion spring positioned between the Pawl and the Lower Part, and a compression spring between the Y-Stirrup and the Ankle Component, simulating the dynamic behaviour of the stance control mechanism under external loads.

A load of 39N was applied at the bottom of the foot plate, 180mm away from the ankle joint centre. Uprights were given fixed support. Figure 4 represents the boundary conditions used in this first rigid body dynamics analysis and materials used are listed in table 3.

The governing differential equation for the rigid body dynamics of a structure [15]:

$$[M] \{\ddot{\delta}\} - [K] \{\delta\} = \{F\}$$

Here [M] represents mass matrix, [K] shows the stiffness matrix, [F] is force matrix, {δ} displacement vector and {$\ddot{\delta}$} acceleration vector.

A second rigid body analysis was performed by introducing a rotational displacement of 4.7° to the Y-stirrup. This analysis aimed to further validate the accuracy of the simplified CAD model. The boundary conditions for this second simulation are illustrated in figure 5.

Table 4: Material properties

Material	Mass density (kg/m^3)	Young's modulus (GPa)	Poisson's ratio	Ref
SS 304	7900	193	0.29	[24]
SS 410	7750	200	0.28	[25]

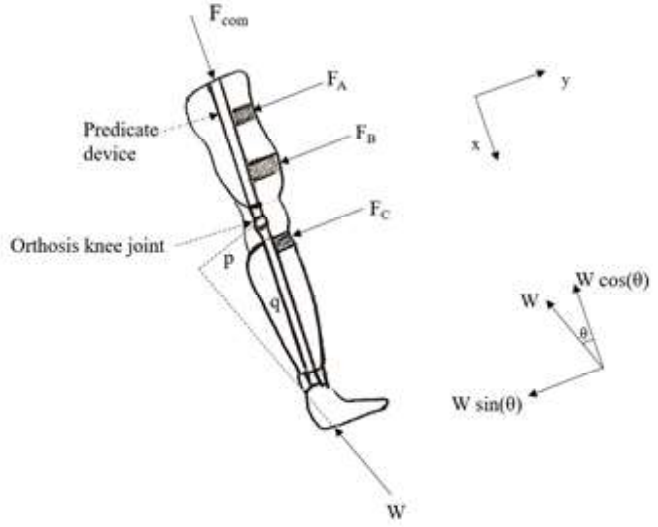

Figure 6: Free body diagram

The material properties for Polypropylene, Fe 4140, and Stainless Steel were obtained from the ANSYS material library. Properties for SS410 and SS304, are provided in table 4.

Maximum theoretical force acting on the orthosis knee joint

Figure 6 illustrates the free body diagram and position of the leg with the orthosis between the heel strike and the loading response phase of gait. The leg position was assessed at a moment arm length of 44 mm from the knee joint [10]. The reaction force was assumed to act at the straps of the orthosis, opposing the leg's motion. The orthosis features three straps, with their positions are shown in figure 7. To calculate the maximum load acting on the orthosis, the running condition was taken into account. Running

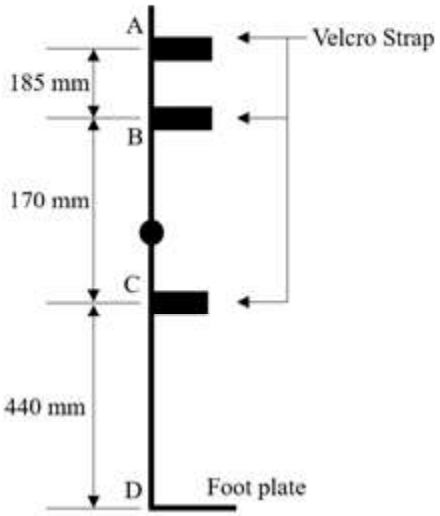

Figure 7: Position of the Velcro straps on the orthosis used for strap load calculations

can generate ground reaction forces reaching up to 2.8 times a person's body weight [11]. According to Anderskey et al., the orthosis transfers 30% to 83% of the limb load away from the user [12]. For a user weighing 60 kg, the estimated ground reaction force during running was approximately 1648 N, resulting in a maximum load of 1367.84 N being transferred to the orthosis. This value was taken as the effective ground reaction force for subsequent calculations.

Using the moment arm length (p) and the length from the foot plate to the knee joint (q) is 491 mm, the angle of the ground reaction force (è) was calculated as 5.141°.

Considering the static equilibrium conditions, the sum of forces acting in the vertical direction was zero and F_{com} (figure 6) was calculated to be approximately 1362 N. The sum of forces in the horizontal direction and the sum of moments about point A were also zero. The system was statically indeterminate, with two equations and three unknowns, and was solved using the method of redundant reactions [13]. Reaction forces acting on the straps were calculated as: F_A = 265 N, F_B = - 235.02 N, and F_C = -152.98 N.

To evaluate the highest forces acting on the orthosis mechanical knee joint in the x, y, and z axes, a structural simulation was conducted. In this analysis, the foot plate was constrained to simulate ground contact, all inter-component connections are modelled as fixed, and the applied forces are illustrated in figure 8. Table 3 lists the components and their respective materials used in this analysis. The material properties of polypropylene were obtained from ANSYS material library, and the properties of SS410 and SS304 are provide in table 4. The forces at the knee joint were determined by analysing the reaction forces at the connection between the upper and lower knee joint segments.

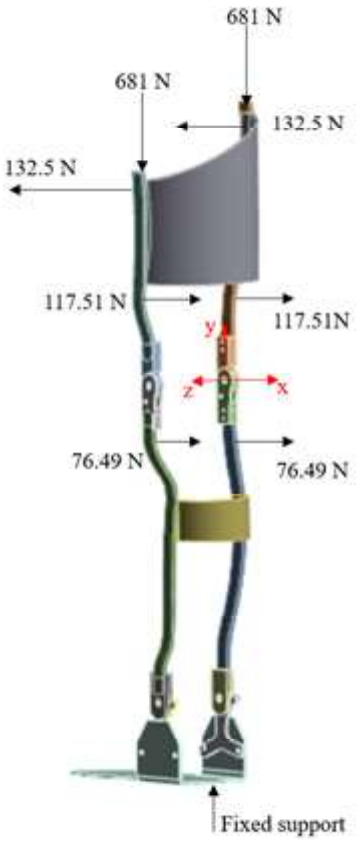

Figure 8: Boundary conditions

Static structural analysis under maximum theoretical loading condition

The static structural analysis of the knee joint was performed using ANSYS to evaluate the stress response under the maximum theoretical loading condition. The model constrained the upper and lower regions of the knee joint, corresponding to the fixed uprights. Applied forces of 21.74 N, 862.99 N, and -35.89 N acted along the x, y, and z axes, respectively, as depicted in figure 11(a). The material properties of SS410 are provide in table 4.

The finite element model equations for the structural response of predicate device under static loading are [15]:

$$[K] \{u\} = \{F\}$$

Where [K] represents the stiffness matrix, {u} is the displacement vector and {F} shows the force vector.

Static structural analysis under practical loading condition

The analysis was conducted to assess the stress response of predicate knee joint under the maximum practical loading condition. According to Anderskey et al., the maximum force acting on the KAFO knee joint occurs during fast walking on a pebble gravel surface [6]. For a 60 kg user, the recorded forces were 28.14 N (x-direction), 234.42 N (y-direction), and 37.80 N (z-direction). The analysis constrained the upper and lower regions of the knee joint, simulating the fixed uprights. The applied forces and boundary conditions are illustrated in figure 12(a), table 4 summarizes the material properties used.

Results

Material identification of predicate device

The elemental composition of the predicate device components and the alloy identification were performed by using a handheld XRF analyser. The XRF analysis revealed that the upper and lower parts of the predicate device were made of Stainless Steel 410 (SS410). The uprights and ankle component were identified as Stainless Steel 304 (SS304), which is an austenitic stainless steel. The pawl was found to be made of Fe 4140, a chromium-molybdenum alloy steel (table 3). XRF spectra of different components of the predicate device along with their percentage elemental compositions are given in figure 9.

Measurement of unlocking force via foot load application

In this experiment, force was applied to the foot with a load cell positioned 180 mm from the ankle joint centre. An average force of 38.98±1.74 N is necessary to rotate the pawl by 4°, thereby reaching the unlocking position.

Measurement of unlocking force via direct cable loading

In this experiment, force was applied directly to the pawl. A force of 20.69±0.82 N was sufficient to rotate the pawl by 4°, achieving the unlocking condition.

The predicate device incorporated a torsion spring at the pawl mechanism to assist in re-locking. Experimental tests showed that a force of 20.69 N was required to rotate the pawl by 4°. Using this data, the stiffness of the torsion spring was determined based on the relation:

$$K = T/\theta$$

where K represents torsion spring stiffness, T denotes applied torque and θ represents angle of rotation.

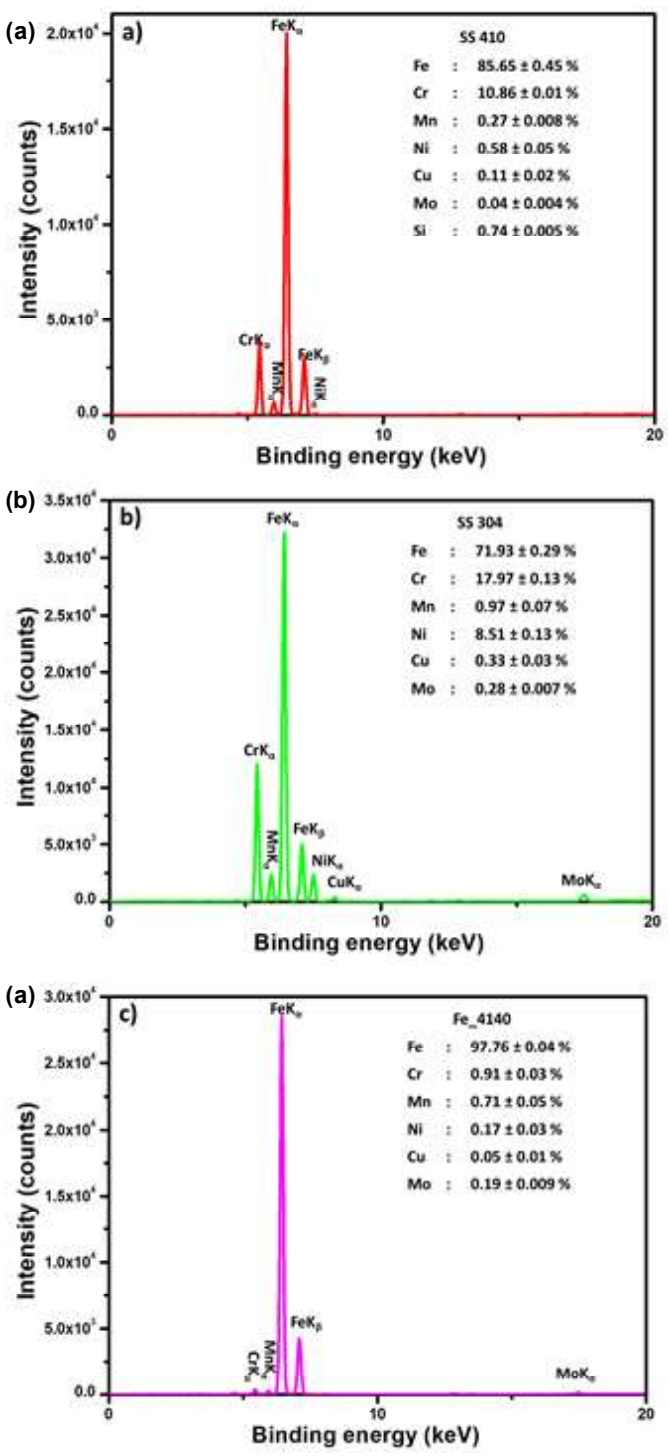

Figure 9: XRF spectra of a) Upper part, b) ankle component and c) pawl of predicate device

By applying this relation, torsion spring stiffness was calculated to be approximately 181 N·mm/°.

In the predicate device, a compression spring was integrated at the Y-stirrup, positioned 13.9 mm from the ankle joint centre, with a cable attachment located 30 mm away from ankle joint centre (figure 10). When a load of 39 N was applied at the foot, it generated a

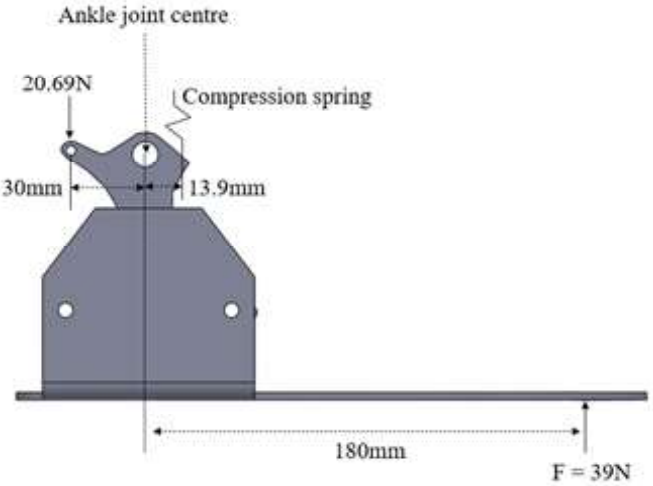

Figure 10: Orthosis CAD model showing the Y-stirrup with compression spring

moment at the ankle joint, which was resisted by the compression spring. Based on the resulting cable force 20.69 N, the spring force was estimated to be 208 N. A 4° pawl rotation corresponded to a 4.7° rotation of the Y-stirrup, resulting in a spring compression of 1.139 mm. The stiffness of the compression spring was determined using the relation:

Where K represents the stiffness of the spring, F denotes the applied force, and x represents the resulting displacement of the spring. The stiffness of the compression spring was calculated to be approximately 183 N/mm.

Rigid body analysis

A load of 39 N applied at the foot of the orthosis turns the pawl by 4.16° and generates a force of 21.51 N at the pawl. When y stirrup rotates through 4.7°, the joint force at the pawl cable point was found to be 20.28 N and the moment at the knee ankle joint

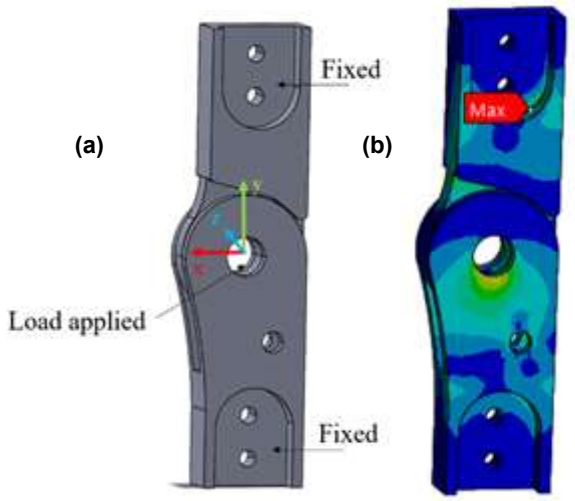

Figure 11: (a) Boundary condition (b) Stress distribution of predicate knee joint under theoretical loading condition

Table 5: Comparison of experimental and rigid body simulation results

Test Scenario	Experiment result	Rigid body simulation result	Error percentage
Force required at the foot of the orthosis to rotate the pawl by 4°	38.98 N	40 N	2.61%
Force at pawl cable point to rotate the pawl by 4° when 39N is applied at the foot of the orthosis	20.69 N	21.51 N	3.96%

was found to be 714.07 N.mm. And the corresponding compression of linear spring is 1.13mm.

An analytical method was used to find the load required at the foot of the orthosis to produce the simulated ankle joint moment of 714.07 N·mm. A force applied 180 mm from the ankle joint created a dorsiflexion moment, opposed by a compression spring (stiffness: 183 N/mm) located 13.9 mm from the ankle joint. When the Y-stirrup spring compressed by 1.139 mm, it generated a resisting force of 208 N. Considering the net moment at the ankle joint centre, the required force at the foot was estimated to be approximately 20 N for one side of the orthosis. Since the orthosis includes ankle and knee components on both the left and right sides, the total required force was approximately 40 N. Experimental measurements showed that the actual force required was 38.98 N, indicating a close match with the theoretical estimation and validating the accuracy of the simplified 3D model. The comparison of experimental and rigid body simulation results is shown in table 5.

Maximum theoretical force acting on the orthosis knee joint

The reaction forces at the junction between the upper and lower segments of the knee joint are analysed, yielding maximum force values of 21.74 N in the x-direction, 862.99 N in the y-direction, and -35.89 N in the z-direction.

Static structural analysis under maximum theoretical loading condition

For the theoretical force, the analysis reveals an equivalent (von Mises) stress of approximately 8.63 MPa (figure 11(b)). At the point where the stress was highest, the principal stresses were determined to be -0.19 MPa (maximum) and -13.23 MPa (minimum).

Static structural analysis under practical loading condition

Under the maximum practical loading condition, the analysis indicates an equivalent stress of approximately 4.70 MPa (figure 12(b)). At the point where the stress is highest, the principal stresses were determined to be -1.41 MPa (maximum) and -6.81 MPa (minimum).

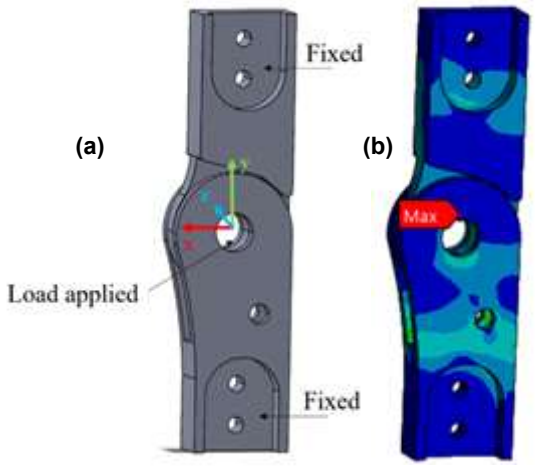

Figure 12: (a) Boundary condition (b) Stress distribution of predicate knee joint under practical loading condition

Discussion

X-ray Fluorescence analysis verified that the materials used in the orthotic components were consistent with those reported in existing literature.

A difference of approximately 3.96% was observed between the experimental and theoretical results for the force required at the pawl cable, and a difference of 2.61% was observed for the force required at the foot of the orthosis. This variation is likely due to factors such as cable stretch, joint play, consideration of simplified CAD model. The simplified 3D CAD model was validated against experimental results, confirming that it can be used for analysis driven design of mechanical knee joints of SCKAFO.

In the FEA analysis, the maximum equivalent stress under the theoretical loading condition was observed at the upper part of the knee joint. By comparing the maximum and minimum principal stresses at this location, it was found that the stresses were low and compressive in nature, indicating that the material is unlikely to fail under this loading condition. During practical loading, the highest equivalent stress in the knee joint occurred near its upper region. Principal stress evaluation at this point showed low compressive values, suggesting that the material remains structurally safe under practical loading scenarios.

Conclusions

This study evaluated the structural and unlocking performance of the predicate device. Experimental tests identified the force needed to unlock the joint, while multibody simulations rigid body dynamic simulation models were verified with experimental results. Finite element analysis showed that the knee joint remains structurally safe under both the theoretical and practical loading condition.

Acknowledgement

The authors gratefully acknowledge the support provided by the Technology Intervention for Disabled and Elderly (TIDE) program of the Department of Science and Technology (DST), Government of India, through extramural funding (Grant No. SEED/TIDE/2019/534). This work was supported by many divisions/departments of the Sree Chitra Tirunal Institute for Medical Sciences & Technology, Trivandrum.

References

1. Kumar A, Vinita. Current Status of Prosthetic and Orthotic Rehabilitation Services in India: Its Issues and Challenges. Front Health Inform. 10(1), 55 (2021).
2. Terris Yakimovich, Edward D. Lemaire, Jonathan Kofman, Engineering design review of stance-control knee-ankle-foot orthoses. 46(2), 257-6 (2009).
3. Ontario Health (Quality). Stance-Control Knee-Ankle-Foot Orthoses for People With Knee Instability: A Health Technology Assessment. Ont Health Technol Assess Ser. 21(11), 1-96 (2021).
4. Raijmakers B, Brehm MA, Nollet F, Koopman FS. Safety, walking ability, and satisfaction outcomes of the NEURO TRONIC stance-control knee-ankle-foot orthosis (SCKAFO): A comparative evaluation to the E-MAG active SCKAFO. Prosthet Orthot Int. 48(1), 30-38 (2024).
5. Pröbsting E, Kannenberg A, Zacharias B. Safety and walking ability of KAFO users with the C-Brace® Orthotronic Mobility System, a new microprocessor stance and swing control orthosis. Prosthet Orthot Int. 41(1), 65-77 (2017).
6. Andrysek J, Klejman S, Kooy J. Forces and moments in knee-ankle-foot orthoses while walking on irregular surfaces: a case series study. Prosthet Orthot Int. 38(2), 104-13 (2014).
7. Khan, S & Zaidan, M & Tajul, Liyana. Lightweight design of Knee-Ankle-Foot Orthotic Devices using Voronoi patterns for Additive Manufacturing. Journal of Physics: Conference Series. 2643. 012007 (2023).
8. Gerez LF, Vieira AFC. Design of an adjustable stance-control knee-ankle-foot orthosis for pediatric population. J Pediatr Rehabil Med. 12(3), 305-312 (2019).
9. Josep M. Font-Llagunes, Rosa Pàmies-Vilà, Javier Alonso, Urbano Lugrís. Simulation and design of an active orthosis for an incomplete spinal cord injured subject, 2, 68-81 (2011).
10. Hunt MA, Birmingham TB, Giffin JR, Jenkyn TR. Associations among knee adduction moment, frontal plane ground reaction force, and lever arm during walking in patients with knee osteoarthritis. J Biomech. 39(12), 2213-20 (2006).
11. Kluitenberg B, Bredeweg SW, Zijlstra S, Zijlstra W, Buist I. Comparison of vertical ground reaction forces during overground and treadmill running. A validation study. BMC Musculoskelet Disord. 13, 235 (2012).
12. Andrysek J, Redekop S, Matsui NC, Kooy J, Hubbard S. A method to measure the accuracy of loads in knee-ankle-foot orthoses using conventional gait analysis, applied to persons with poliomyelitis. Arch Phys Med Rehabil. 89(7), 1372-9 (2008).
13. Hardy Cross. Statically Indeterminate structures. D-J Multi Print CO. (1926).
14. Michael W. White. Gait Analysis An Introdcution. Elsevier Limited (2007).
15. P. Seshu. Text Book of Finite Element Analysis. PHI Learning Private Limited (2012).
16. Becker Orthopedics (n.d.) Ankle Components [Brochure].
17. Becker Orthopedics. Stride Family [Brochure]. (2012).
18. Becker Orthopedics. Stride Family Kits Ordering Information [Brochure]. (2015).
19. Becker Orthopedics. FullStride SafetyStride Fabrication Instruction [Brochure]. (2021).
20. Fior & Gentz. Materials [Brochure]. (2024).
21. Fior & Gentz. NEURO MATIC [Brochure]. (2024).
22. Fior & Gentz. System Joints and Articulate System Side Bars [Brochure]. (2017).
23. Endolite India Limited. High technology prosthetic & orthotic products [Brochure].
24. Atlas Steels, Stainless Steel Grade Datasheets, data sheets, 2011.
25. Azo Materials. Stainless Steel - Grade 410, 970 sheet ID.